sciendo

Polish Journal of Chemical Technology, 26, 2, 77—85, 10.2478/pjct-2024-0021

Preparation of efficient hydrochloric acid corrosion inhibitor from natural grease

Yi Luo[1, 2], Zhongying Xu[1, 3#], Xuewen Cao[3], Yefei Wang[3], Shanjian Li[1], Gang Chen[2], Ying Tang[1, 2*]

[1]Engineering Research Center of Oil and Gas Field Chemistry, Universities of Shaanxi Provence, Xi'an Shiyou University, Xi'an, 710065, China

[2]Shaanxi Province Key Laboratory of Environmental Pollution Control and Reservoir Protection Technology of Oilfields, Xi'an Shiyou University, Xi'an, 710065, China

[3]China University of Petroleum (Huadong), Qingdao, 266580, China

Co-first author

[*]*Corresponding author: e-mail:* tangying78@xsyu.dedu.cn

To alleviate the metal corrosion problem caused by incomplete acid discharge during pickling or acidification, a corrosion inhibitor, long chain fatty hydrazides (LCFH), with a significant corrosion inhibition effect was synthesized from natural grease. The corrosion inhibition and adsorption properties of LCFH on carbon steel in 1 M HCl solution were studied by static sample weight loss test, electrochemical impedance spectroscopy, and potentiodynamic polarization curve. The results showed that LCFH exhibits excellent corrosion inhibition performance in HCl solution. The inhibition efficiency increases with the increase of inhibitor concentration. When the concentration of LCFH is 40 mg/L, the inhibition efficiency can reach 97.9%. The potentiodynamic polarization curve shows that LCFH is a corrosion inhibitor that mainly inhibits the cathodic reaction. The corrosion inhibitor is spontaneously adsorbed on the surface of low-carbon steel in physical form, which conforms to the Langmuir isothermal adsorption model.

Keywords: Acidic corrosion; Long chain fatty hydrazides; Corrosion inhibitor; Natural grease.

INTRODUCTION

In oil exploration and drilling operations, acidic solutions (HCl solution and H_2SO_4 solution) are often used to clean pipelines and steel frames, dissolve blockages in cracks or expand the original pores and cracks that connect oil and gas layers, increase the permeability of oil and gas layers, and reduce oil and gas seepage resistance, thereby increasing the production of oil and gas wells[1–3]. Therefore, it is very important to inhibit metal corrosion. At present, the main methods to inhibit metal corrosion include the use of corrosion-resistant steel[4], electrochemical protection[5], coating treatment of metal surface[6], and the addition of corrosion inhibitors[7]. Since other protection methods are either inefficient or costly, corrosion inhibitors are agents that can effectively slow or prevent metal corrosion by adding only a small amount. Therefore, adding corrosion inhibitors is the most commonly used method to inhibit metal corrosion.

The use of organic compounds in the industry has the advantages of excellent corrosion inhibition, cost-effectiveness, ease of application and synthesis, and is more environmentally friendly than inorganic compounds. Most of the organic compounds currently used as corrosion inhibitors contain oxygen, nitrogen, and sulfur elements or multiple bonds, mainly heteroatomic compounds such as amino acids[8], Schiff bases[9], Mannich bases[10], triazine compounds[11], and quaternary ammonium salts[12]. These organic compounds contain π-electrons and heteroatoms that share charges with the empty *d*-orbitals of the metal, that is, the inhibitor molecules will adsorb to the metal surface and occupy the active sites, thereby reducing the corrosion rate[13, 14]. They are also effective under harsh conditions, such as concentrated acid and high temperature[15]. In addition, compounds containing multiple heteroatoms have better corrosion inhibition efficiency than compounds containing only one heteroatom. This is because there are more adsorption centers on the inhibitor molecules with more heteroatoms[16, 17].

In recent years, our research group[18, 19] and other researchers[20–23] have synthesized a series of compounds with multiple bonds and heteroatoms and analyzed the corrosion behavior of mild steel in hydrochloric acid solution at different temperatures by weight loss method, polarization curves, and electrochemical impedance spectroscopy techniques. The mechanism of corrosion was explored by calculation of thermodynamic parameters and adsorption isotherms, all of which have yielded promising results. Among them, not a few researchers have studied the corrosion inhibition of hydrazide derivatives in HCl solutions and found that hydrazide derivatives are good corrosion inhibitors in acid medium[24–27]. However, the previous methods for synthesizing fatty hydrazides had great drawbacks. Either the raw materials are more complicated, or the synthesis method is more complicated, and it is not easy to prepare on-site construction. In the work of Siutkina, A.I., et.al[28], 2-(2-(diarylmethylene) hydrazino) -5,5-dimethyl-4-oxohexane-2-enoylhydrazide was synthesized by ring-opening reaction using 3-diarylmethylene hydrazine-5-tert-butyl-3H-furan-2-one as raw material. In the work of Baleeva N.S.[29], (3-exo, 7-endo) -7-hydroxybicyclo [3.3.1] nonane-3-formylhydrazide was obtained by the reaction of 4-oxahomoadamantane-5-one with hydrazine. These raw materials are not easy to obtain. Therefore, we synthesized a new compound-long chain fatty hydrazides (LCFH) using hydrazine hydrate and canola oil. Canola oil is a necessity in people's daily life. It contains O, N and multiple bonds and is easy to obtain. Hydrazine hydrate is a very common fine chemical product with strong alkalinity and hygroscopicity. It not only has the generality of amines, but also has strong reducibility. It is often used as a deoxidizer in aqueous media. However, since hydrazine hydrate has some toxicity, the reaction between canola oil and hydrazine hydrate is used to reduce the toxicity of hydrazine hydrate. The hydrazine corrosion inhibitors synthesized in this paper meet all the conditions of industrially used corrosion inhibitors.

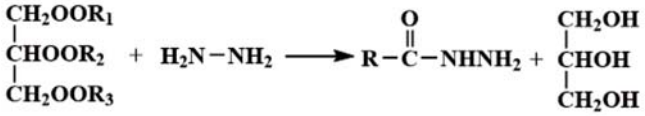
In this paper, LCFH corrosion inhibitor was synthesized by hydrazine hydrate and natural vegetable oil. The corrosion inhibition effect of the composite corrosion inhibitor on low carbon steel in 1 M HCl solution was studied by static weight loss method, polarization curve method, and electrochemical impedance spectroscopy. The adsorption behavior of the composite inhibitor on the metal surface was analyzed by calculating the thermodynamic parameters. The adsorption and action mechanism of the composite inhibitor on mild steel in 1 M HCl solution was explained by electrochemical experiments, which confirmed the experimental conclusion of the static coupon weight loss method.

Experimental details

Materials preparation

Synthesis of hydrazine corrosion inhibitor (LCFH)

One mole of canola oil was added to a three-necked flask and the temperature was set to 80 °C. The mixture was then slowly added to the reactor through a constant pressure-dropping funnel. The mixture was slowly added to the reactor through a constant pressure-dropping funnel. Hydrazine hydrate (2 moles, 57%) was slowly added dropwise to the reactor through a constant pressure dropping funnel while the mixture was magnetically stirred for 4 hours. The synthetic route is depicted in Scheme 1. Where, R_1, R_2, and R_3 represent alkyl groups, and R contains R_1, R_2, and R_3.



Scheme 1. Synthetic route of LCFH

Synthetic route of LCFH

Mild steel sample and corrosive medium

Q235 Mild steel was purchased from Shanghai Mechanical and Electrical Equipment Co., and the coupons, content, and properties of Q235 used in this experiment are shown in Tables 1 and 2. The data in the tables are from the factory inspection report of the steel sheet. The size of Q235 sample for weight analysis is 40×2×13 mm^3. To obtain reliable and accurate research results, all mild carbon steel samples were pretreated, including wiping with different grades (280-360-600-1000) of sandpaper to remove rust particles until the surface of mild carbon steel was smooth without rust. After that, the mild carbon steel was degreased with acetone, then wiped with absolute ethanol, and dried in cold air[30, 31].

The acidification environment was simulated by diluting the analytical grade 9 M HCl acid to 1 M. In addition, the concentrations of the inhibitors used ranged from 10 to 50 mg · L^{-1}.

Table 1. Q235 mild steel sheet composition content

Coupons	C	Si	Mn	P	S	Al	Cr	Ni	Cu
Content (%)	0.16	0.26	0.15	≤0.015	≤0.09	/	0.02	0.025	0.024

Table 2. Q235 mild steel sheet tensile and process properties

Tensile strength (b/MPa)	Yield strength (0.2/MPa)	Elongation (5%)	Density (g · cm^{-3})
425	310	35	7.85

Weight loss measurements

Gravimetric experiments were carried out on mild steel specimens at 303, 313, 323, 333 and 343 K with different concentrations of LCFH starting from 10 mg · L^{-1} and ranging from 20, 30, 40 and 50 mg · L^{-1}. Steel specimens were suspended and immersed in 1 M HCl solution for 4 h. Secondly, the specimens were removed from the solution, rinsed using distilled water and anhydrous ethanol, and dried and the weight loss was calculated based on the difference obtained by weighing before and after immersion. Corrosion loss by weight was used to calculate the average corrosion rate (C_R), and the corrosion inhibition efficiency (η) was calculated as Eqs. 1 and 2[32]:

$$C_R = \frac{M_0 - M_1}{St} \quad (1)$$

$$\eta(\%) = \frac{M_0 - M_1}{M_0} \times 100 \quad (2)$$

Where, M_0 and M_1 (g) are the mass loss values in the presence and absence of LCFH, respectively. S (cm^2) is the surface area of low carbon steel, and t (h) is the soaking time.

SEM analysis

To further investigate the adsorption of corrosion inhibitor on the surface of Q235 steel specimens, the specimens were placed in an un-added and added 1 M HCl solution, corroded at 343 K for 4 h. After removal, the specimens were rinsed with distilled water and anhydrous ethanol, and then blown dry in cold air and then scanned using an electron microscope for electron microscope scanning.

Electrochemical measurements

Electrochemical tests were performed using the CST520 electrochemical workstation of Wuhan Koster Instrument Co., Ltd., using a three-electrode system. The working electrode material is a self-made low-carbon steel electrode, the reference electrode is a saturated calomel electrode, the auxiliary electrode is a platinum electrode, and the corrosion medium is a 1 M HCl solution containing different concentrations of LCFH. Grind the working electrode with sandpaper until the surface is smooth. The electrode surface was rinsed with anhydrous ethanol and installed in a four-necked flask after drying. The effective exposure area was 1 mm^2. The open circuit potential scanning time is 20 min, and the open circuit potential change within 5 min is stable at ±5~10 mV, and subsequent tests can be performed after stabilization.

(1) Potentiodynamic polarization curve scanning: Potentiodynamic polarization curve scanning is to select the dynamic potential scanning in the steady-state test

in the test method, in which the scanning range is open circuit potential ±250 mV, and the scanning speed is 0.5 mV/s[33, 34].

(2) Electrochemical impedance spectroscopy scanning: The AC impedance measurement method is to measure the impedance spectrum of the system at different frequencies through the impedance-frequency scanning curve. The Nyquist and Bode diagrams are generally used to represent the impedance spectrum. The frequency range of the impedance spectrum is set to 0.01 Hz~100 kHz, and the amplitude of the excitation sine wave signal is 10 mV[35].

RESULTS AND DISCUSSION

FT-IR analysis

It can be seen from the spectrum (Fig. 1) that the strong and wide peak at 3320 cm^{-1} was O-H stretching vibration, and the strong and wide peak at 1743 cm^{-1} was C=O stretching vibration, indicating that the compound contained esters. In the wave number range of 1640–1515 cm^{-1}, it is generally the N-H deformation vibration frequency region of hydrazine, and the peak near 700 cm^{-1} represents the N-H out-of-plane deformation vibration of hydrazine. Therefore, it can be explained that LCFH was successfully synthesized.

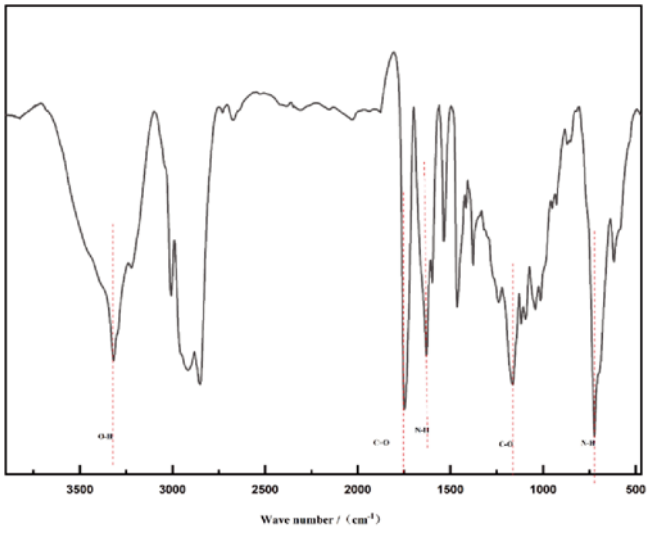


Figure 1. Infrared spectrum of LCFH

Weight loss measurements

In the hydrazinolysis reaction, the reaction temperature has a certain influence on the corrosion inhibition performance of the composite inhibitor. In this experiment, mild steel was used as the test piece, and 1 M HCl solution was used as the corrosion medium. The temperature of the constant temperature water bath was set to 303, 313, 323, 333 and 343 K, respectively. The corrosion rate of steel under different temperature conditions was determined as shown in Figure 2.

It can be seen from Figure 2 that at room temperature, the corrosion inhibition rate increases with the increase of inhibitor concentration. the adsorption capacity of its molecules on the steel surface increases and the specific surface area of the protective film formed on the metal surface increases.

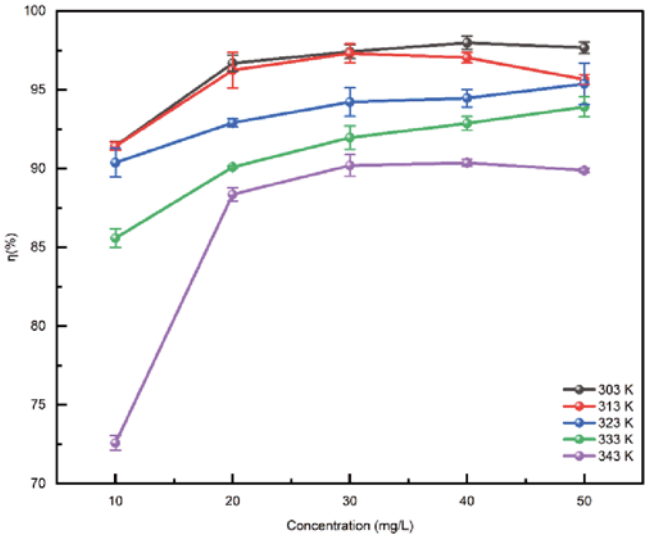


Figure 2. The inhibition rate of corrosion inhibitor at different temperatures

It can also be seen from Figure 2 that when the LCFH concentration is the same, the higher the temperature is, the lower the corrosion inhibition rate is. At the LCFH concentration of 20 mg/L, there is a sudden decrease in the corrosion inhibition rate at each temperature, after which the corrosion inhibition rate does not change much as the LCFH concentration rises, so from the perspective of environmental protection and economy, the best LCFH concentration is 20 mg/L, when the corrosion inhibition rate is almost always at more than 90%. In the case of hydrazide derivatives, as corrosion inhibitors studied in recent years, few corrosion inhibitors can achieve such corrosion inhibition at such low concentrations under the same conditions[36, 37].

SEM analysis

The surface morphology of Q235 steel was observed by scanning electron microscopy under the condition of corrosion in 343 K, 1 M HCl solution for 4 h. The scanning results of Q235 steel in the blank group (a) and when it contained 50 mg/L LCFH (b) are shown in Figure 3.

Figure 3 (a) and (b) are contrasted. It is evident that the steel plate in the blank group is severely corroded and has a mottled surface with rust. In contrast, after adding LCFH to the corrosive medium, the surface of the steel plate remains smooth and uniform after corrosion, with only traces of sandpaper polishing and reduced pitting corrosion. This indicates that LCFH has excellent corrosion inhibition effect on Q235 steel.

Adsorption isotherm and thermodynamic parameters

It was found that the adsorption of LCFH on mild steel surface obeys Langmuir adsorption isotherm equation as Eq. 3:

$$\frac{\theta}{1-\theta} = K_{ads} C_{inh} \tag{3}$$

Eq. 4 is obtained after integration:

$$\frac{C_{inh}}{\theta} = \frac{1}{K_{ads}} + C_{inh} \tag{4}$$

Where C_{inh} (mol/L) represents the concentration of LCFH added to the HCl solution. K_{ads} represents the equilibrium constant in the adsorption process. θ is the

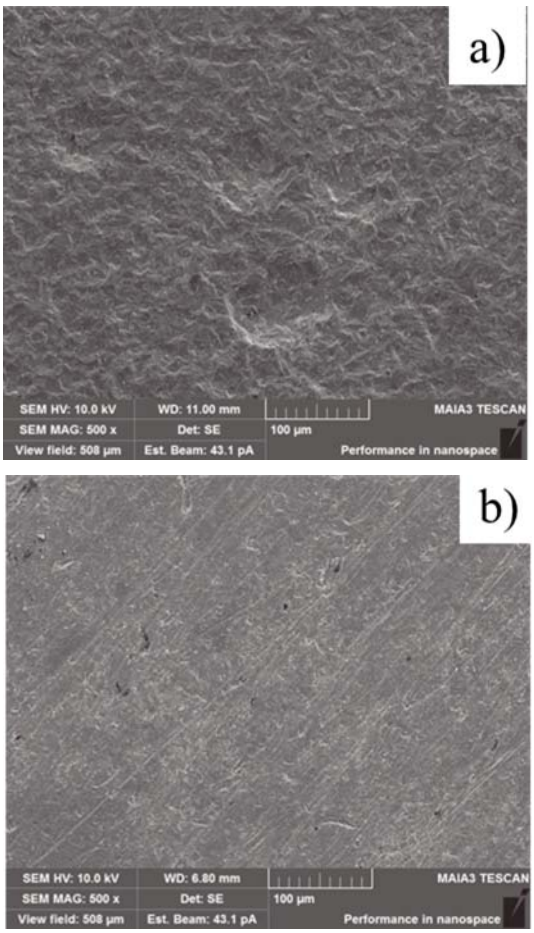


Figure 3. SEM analysis of steel sheet

surface coverage, which is equated to the corrosion inhibition rate in this calculation[38]. According to Eq. 5, its value is related to the standard free energy of adsorption ΔG^0_{ads}.

$$K_{ads}=\frac{1}{55.5}exp(\frac{-\Delta G^0_{ads}}{RT}) \quad (5)$$

Where, R represents the molar constant of gas, which is 8.3145 J/mol/K. T (K) is the thermodynamic temperature. 55.5 mol/L is the concentration of water molecule[39]. Figure 4 is the Langmuir adsorption isotherm of LCFH molecules on mild steel surface at different temperatures in 1 M HCl solution. As shown in Table 3, R^2 was 0.99, indicating that the experimental data can be described by Langmuir isotherm[40]. The K_{ads} can be calculated from the intercept between the straight line and the C_{inh}/θ-axis, as shown in Table 3, and the ΔG^0_{ads} calculated from Eq. 5, which is also shown in Table 3.

In general, when the absolute value of ΔG^0_{ads} is lower than 20 kJ/mol, it is related to physical adsorption, when it is higher than 40 kJ/mol, it is related to chemical adsorption, and when it is between 20 kJ/mol and 40 kJ/mol, it is related to the mix of physical adsorption and chemical adsorption. This is due to the formation of coordination bonds between organic molecules to share or transfer electrons to the metal surface[41]. The calculated absolute value of ΔG^0_{ads} is between 20–30 kJ/mol, indicating that the inhibition mechanism of LCFH on low carbon steel in 1 M HCl solution is the coexistence of chemical adsorption and physical adsorption. However, we found that the absolute value of ΔG^0_{ads} decreases with the increase of temperature, which indicates that with the increase of temperature, the adsorption of corrosion inhibitor molecules on the metal surface is unfavorable, which indicates that physical adsorption contributes more to the adsorption process.

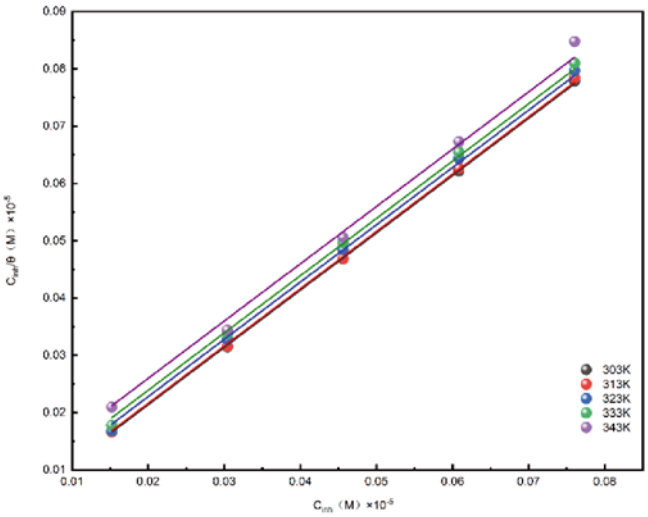


Figure 4. Langmuir isothermal adsorption model of LCFH molecules on mild steel surface at different temperatures in 1 M HCl solution

Table 3. Adsorption thermodynamic parameters of LCFH on sheet at different temperatures

Temperature (K)	K_{ads}	R^2	ΔG^0_{ads}(kJ/mol)
303	740.74	0.99	–26.76
313	515.00	0.99	–26.70
323	358.42	1	–26.58
333	256.41	1	–26.48
343	189.22	1	–26.40

Thermodynamically, ΔG^0_{ads} is related to ΔH^0_{ads} and ΔS^0_{ads}, respectively. It can be obtained from Eq. 6:

$$\Delta G^0_{ads}=\Delta H^0_{ads}-T\Delta S^0_{ads} \quad (6)$$

The standard adsorption enthalpy (ΔH^0_{ads}) can be calculated according to the *Van 't Hoff* equation. From Eq. 7:

$$lnK_{ads}=-\frac{\Delta H^0_{ads}}{RT}+constant \quad (7)$$

The curve of $\ln K_{ads}$ against $1000/T$ is a straight line, as shown in Figure 4, from whose slope ΔH^0_{ads} can be obtained (ΔH^0_{ads} = –33.21 kJ/mol). The value of adsorption entropy ΔS^0_{ads}(–23.55 J/(mol/K)) can be calculated from Eq. 6. Since the value of ΔH^0_{ads} is negative, it indicates that the adsorption process of the inhibitor molecule is exothermic. The value of ΔS^0_{ads} was negative, indicating that the LCFH molecules moved freely in the solution before adsorption. With the adsorption process going on, the adsorption of LCFH molecules on the surface of mild steel became more orderly, resulting in a decrease in entropy. It can also be understood that as the reaction temperature increases, LCFH gradually adsorbs on the surface of the steel to form a protective film[42].

By comparing with other literature[43, 44], it is found that the LCFH synthesized in this paper has a lower negative value of adsorption enthalpy on the metal surface, which means that the process of desorption of the corrosion inhibitor molecules from the mild steel surface needs to absorb higher energy to complete, which means that this corrosion inhibitor is more stable and can occupy

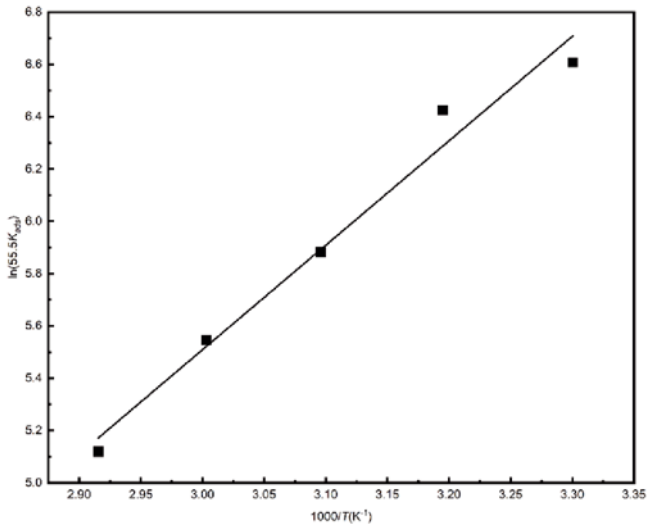


Figure 5. *Van't Hoff* diagram for the mild steel

the active site more effectively, thus inhibiting the corrosion of metals.

Effect of temperature

We can see from Figure 5 that the corrosion rate decreased with the increase of the temperature. This is due to the increased rate of dissolution process of mild steel and partial desorption of the inhibitor from the metal surface with temperature. To calculate the thermodynamic parameters of the corrosion process, the Arrhenius formula (Eq. 8) was used[45].

$$C_R = A\ exp(-\frac{E_a}{RT}) \tag{8}$$

After deformation, Eq. 9 and Eq. 10:

$$lnC_R = lnA - \frac{E_a}{RT} \tag{9}$$

$$C_R = \frac{RT}{Nh} exp(\frac{\Delta S_a}{R}) exp(-\frac{\Delta H_a}{RT}) \tag{10}$$

Where, A is pre-exponential factor, E_a is the apparent activation energy, h is the *Plank's* constant, the value is 6.63×10^{-34} J · S, N is the *Avogadro's* constant, the value is 6.02×10^{23} mol^{-1}, ΔS_a is the activation entropy, ΔH_a is the activation enthalpy.

The Arrhenius plot of the corrosion rate of mild steel is shown in Figure 6. The E_a value is determined by the lnC_R against 1000/T diagram. From the slope of lnC_R against 1000/T diagram, the apparent activation energy (E_a) values of mild steel with and without different concentrations of LCFH in the HCl acid solution were determined, as shown in Table 4. E_a decreases with the increasing of inhibitor con-centration. With the increase of temperature, the adsorption amount of LCFH molecules on the surface of the steel decreased significantly, while the desorption amount increased gradually and the activation energy increased. The pre-exponential factor A has a similar trend with the apparent activation energy.

Figure 7 shows the curve of ln (C_R/T) against 1000/T, the slope is (-ΔH_a/R), and the intercept is (ln$R$/Nh+ΔS_a/R), from whom we can calculate the value of ΔH_a and ΔS_a (listed in Table 4). The results show that in 1 M HCl solution, the ΔH_a value (0.46 ~ 10.09 kJ/mol) in the presence of LCFH is lower than that in the absence of LCFH (30.96 kJ/mol). The positive reaction ΔH_a reflects that the dissolution process of mild steel is endothermic,

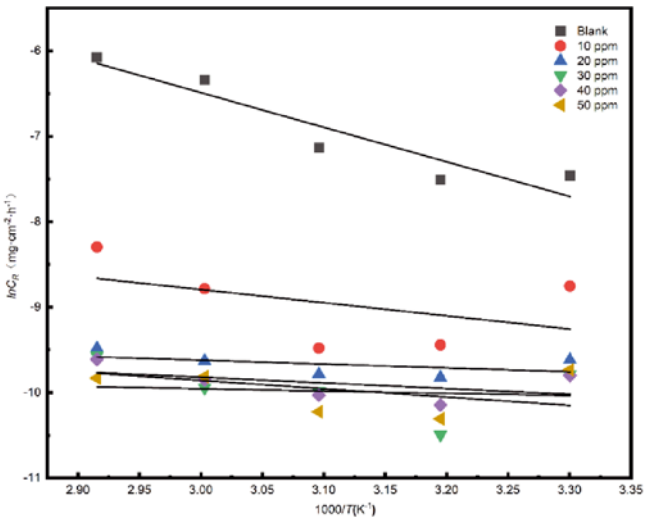


Figure 6. Arrhenius plot of corrosion rate (lnC_R) of mild steel in the presence and absence of LCFH in 1 M HCl solution

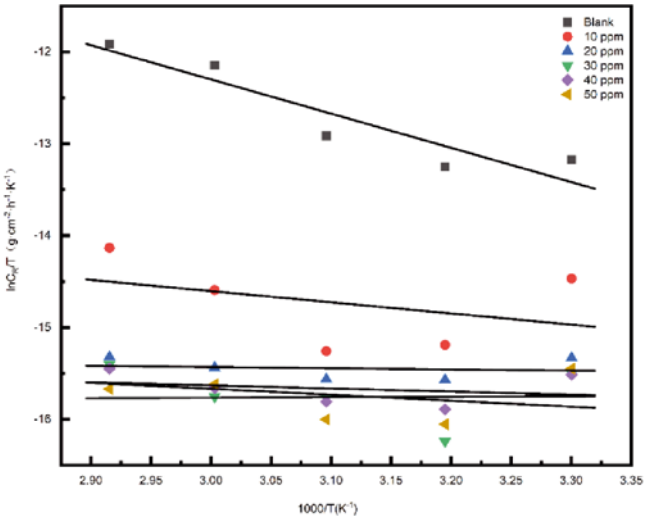


Figure 7. Corrosion rate (C_R) of mild steel in 1 M HCl solution in the presence and absence of LCFH

indicating that the dissolution of mild steel is slow in the presence of LCFH. It can be noted that E_a and ΔH_a values change in the same way.

$$\Delta H_a = E_a - RT \tag{11}$$

The negative entropy indicates that the order from reactants to activated complexes is enhanced. In addition, the value of ΔS_a in HCl solution containing inhibitor is higher than that in HCl solution without inhibitor. This behavior can be reflected in the replacement process of water molecules in the adsorption process of LCFH on the surface of the sheet. With the increase of LCFH concentration, more and more LCFH molecules are adsorbed on the surface of the sheet, which is shown as more and more orderly. The result shown numerically

Table 4. Corrosion kinetics parameters of steel in the presence and absence of LCFH

Concentration (mg/L)	E_a (kJ/mol)	ΔH_a (kJ/mol)	ΔS_a (J/mol·K)
Blank	33.64	30.96	–206.93
10	12.77	10.09	–288.71
20	3.77	1.09	–322.58
30	8.09	5.42	–311.55
40	5.48	2.79	–319.11
50	2.21	0.46	–330.01

is that the absolute value of increases with the increase of LCFH concentration[46].

Electrochemical measurements

Potentiodynamic polarization curves

The experiment was carried out at 30 °C under normal pressure. With 1 M HCl solution as the corrosion medium and LCFH as the corrosion inhibitor, the polarization curves of samples at different concentrations of LCFH were measured, the results are shown in Figure 8. The electrochemical parameters after polarization curve fitting are shown in Table 5.

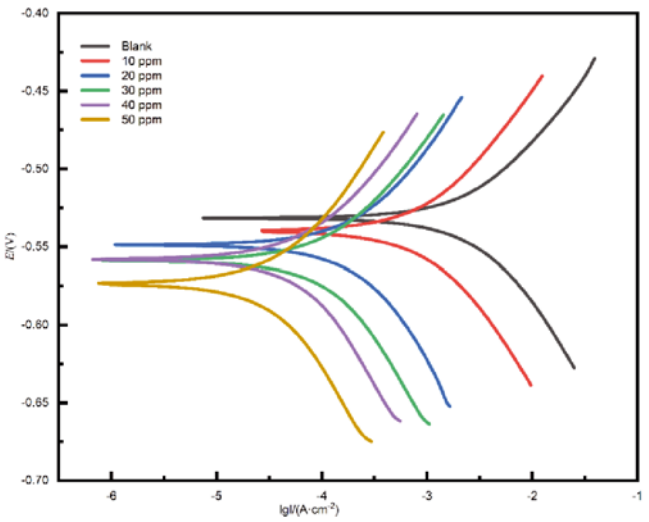


Figure 8. Polarization curves for the sheets in HCl medium for different concentrations of LCFH at 303 K

It can be seen from Figure 8 that with the increase of inhibitor concentration, the cathode area and anode area of the polarization curve move to the low current direction, indicating that the hydrazine inhibitor has an inhibitory effect on both cathode and anode corrosion. With the increase of inhibitor concentration, the self-corrosion potential gradually shifts to negative, indicating that the inhibitor is the inhibitor mainly inhibiting cathodic corrosion.

Table 5 shows the electrochemical corrosion kinetic parameters: corrosion potential (E_{corr}), anode *Tafel* slope (β_a) and cathode Tafel slope (β_c) and corrosion current density (I_{corr}) obtained by extrapolation. The inhibition efficiency *IE* (%) can also be calculated by Eq. 12, where i^0_{corr} is the corrosion current density without LCFH, and I_{corr} is the corrosion current density with LCFH:

$$IE(\%)=\frac{i^0_{corr}-i_{corr}}{i^0_{corr}}\times 100 \quad (12)$$

From the results in Table 5, it can be clearly seen that the Tafel slope of the anode and cathode gradually increases with the increase of the concentration. The corrosion current density decreased from 3.30 μA · cm^{-2} to 0.05 μA · cm^{-2}, and the corrosion inhibition efficiency increased gradually, which was in line with the trend of static weight loss experiment. At a concentration of 50 mg · L^{-1}, LCFH showed the largest inhibition rate (98.42%).

Electrochemical impedance spectroscopy

The impedance spectra of hydrazine inhibitors with different concentrations at 303 K are shown in Figure 9. It can be seen that after adding different concentrations of LCFH, the impedance spectra of low carbon steel show the shape of single capacitance arc. With the increase of LCFH concentration, the radius of capacitive arc increases gradually. Since a single semicircle indicates that the charge transfer process occurs at the electrode--electrolyte interface, it can be shown that the corrosion reaction of low carbon steel is controlled by the charge transfer process. In the high frequency region of the impedance spectrum, the electrode reaction is controlled by the charge transfer process. Therefore, the higher the value of *Rp*, the more difficult it is to corrode[47, 48].

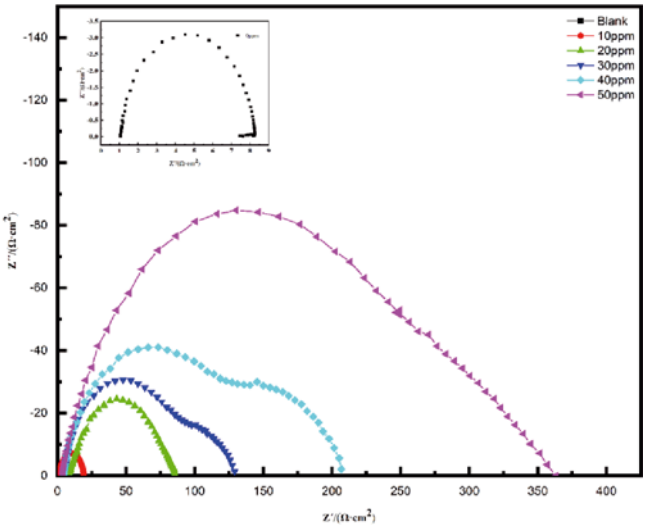


Figure 9. Impedance diagrams of LCFH with different concentrations

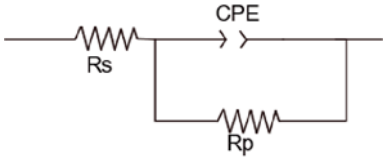


Figure 10. Electrochemical equivalent circuit for metal-electrolyte interface

$$E_{R_p}=\frac{R_p-R^0_p}{R_p}\times 100\% \quad (13)$$

As shown in Figure 10, the experiment is carried out by appropriate equivalent circuit simulation. The standard Randles circuit is used to analyze the impedance spec-

Table 5. Fitting results of polarization curve parameters

Concentration(mg/L)	β_a/mV	β_c/mV	I_{corr} (μA · cm^{-2})	E_{corr} V	IE %
0	92.76	105.96	3.30	–0.53	–
10	63.36	67.89	0.24	–0.52	92.73
20	109.93	136.27	0.30	–0.55	90.91
30	94.39	130.50	0.15	–0.56	95.45
40	94.94	142.03	0.09	–0.56	97.27
50	108.59	148.21	0.05	–0.57	98.42

Table 6. Equivalent circuit fitting data of LCFH with different concentrations

Concentration (mg/L)	Rs ($\Omega \cdot cm^{-2}$)	CPE-T ($\mu F \cdot cm^{-2}$)	CPE-P ($\mu F \cdot cm^{-2}$)	Rp ($\Omega \cdot cm^{-2}$)	E_{R_p} %
0	1.08	3.9×10^{-4}	0.93	7.0	–
10	1.15	5.3×10^{-4}	0.85	17.6	60.19
20	7.85	5.5×10^{-4}	0.68	78.1	91.02
30	4.39	2.9×10^{-4}	0.74	110.9	93.68
40	3.90	2.6×10^{-4}	0.71	174.4	95.98
50	3.75	1.2×10^{-4}	0.7	309.0	97.73

trum including a single capacitor semicircle. The circuit is composed of solution resistance (*Rs*), charge transfer resistance (*Rp*) and phase-fixed element (*CPE*). In order to accurately fit the experimental data, the impedance data are analyzed on the basis of the equivalent circuit diagram, and the results are shown in Table 6. Then, the inhibition efficiency obtained from the impedance measurement is calculated according to Eq. 13, where *Rp* and Rp^0 are the charge transfer resistances in the presence and absence of LCFH, respectively. E_{Rp} represents the corrosion inhibition efficiency in impedance calculation. The *Rp* value increased with the improvement of LCFH concentration. However, the *CPE-P* value tends to decrease. The decrease of *CPE-P* value is due to the adsorption of corrosion inhibitor on the metal surface, which leads to the extension of the thickness of the electric double layer and the decrease of the dispersion index on the metal surface, which further indicates that the corrosion inhibition effect of LCFH gradually increases with the increase of concentration[49].

CONCLUSIONS

All the experimental results show that the corrosion rate of mild steel in HCl solution decreases with increasing LCFH concentration and increases with increasing temperature, but the calculated results show that the maximum corrosion inhibition rate of the corrosion inhibitor reaches 90% even at 70 °C, which shows that the compound has excellent corrosion inhibition effect on mild steel even at high temperature. The adsorption of the compound LCFH on the surface of mild steel is consistent with the Langmuir isothermal adsorption model through adsorption thermodynamic simulations, and its adsorption on the metal surface is spontaneous and dominated by physical adsorption. The polarization curves indicate that the compound LCFH is a corrosion inhibitor that mainly inhibits the cathodic reaction, and the electrochemical impedance spectroscopy tests also support these conclusions. The studied compound is a corrosion inhibitor with excellent inhibition of mild steel corrosion at ultra-low concentrations and can be used in the pickling process at high temperatures.

ACKNOWLEDGMENTS

The work was supported financially by the Key Projects of China National Key R&D Plan (2021YFE0107000), National Natural Science Foundation of China (52074339), Key Scientific Research Project of Shaanxi Provincial Department of Education (21JY035), Xi'an Shiyou University Graduate Innovation Fund Project (YCS22213109) and Youth Innovation Team of Shaanxi University. We also thank the Center of Advanced Analysis and Testing at Xi'an Shiyou University for their work.

LITERATURE CITED

1. Xue, J., Ma, X., Yu, L., Tang, C. & Ma, J. (2012). Development of a novel acidification corrosion inhibitor for P110 steel at high temperature. *Sci. Adv. Mater*. 4(1). DOI: 10.1166/sam.2012.1252.

2. Solomon, M.M., Uzoma, I.E., Olugbuyiro, J.A.O. & Ademosun, O.T. (2022). A censorious appraisal of the oil well acidizing corrosion inhibitors. *J. Petrol. Sci. Eng*. 215(Part B), 110711. DOI: 10.1016/j.petrol.2022.110711.

3. Wang, Q., Zhang, R., Zhang, L., Gao, M., Du, W. & Gu, X. (2021). Preparation of eco-friendly acidic corrosion inhibitors from ilex chinensis sims leaves. *J. Biobased Mater. Bio.* 15(4), 472–477. DOI: 10.1166/jbmb.2021.2090.

4. Ishizaki, T., Masuda, Y. & Sakamoto, M. (2011). Corrosion resistance and durability of superhydrophobic surface formed on magnesium alloy coated with nanostructured cerium oxide film and fluoroalkylsilane molecules in corrosive NaCl aqueous solution. *Langmuir* 27(8), 4780–4788. DOI: 10.1021/la2002783.

5. Khaled, K.F., Hamed, M.N.H., Abdel-Azim, K.M. & Abdelshafi, N.S. (2011). Inhibition of copper corrosion in 3.5% NaCl solutions by a new pyrimidine derivative: electrochemical and computer simulation techniques. *J. Solid State Electrochem*. 15(4), 663–673. DOI: 10.1007/s10008-010-1110-0.

6. S.A. Brown, J.P.S. (2010). Crevice and fretting corrosion of stainless-steel plates and screws. *J. Biomed. Mater. Res*. 15(6), 867–878. DOI: 10.1002/jbm.820150611.

7. Al Juhaiman, L.A., Abu Mustafa, A. & Mekhamer, W.K. (2013). Polyvinyl pyrrolidone as a green corrosion inhibitor for carbon steel in alkaline solutions containing NaCl. Anti-Corros. *Method. Mater.* 60(1), 28–36. DOI: 10.1108/00035591311287429.

8. Chen, G., Yan, J., Liu, Q., Zhang, J., Li, H., Li, J., Qu, C. & Zhang, Y. (2019). Preparation and surface activity study of amino acid surfactants. *C.R. Chim*. 22(4), 277–282. DOI: 10.1016/j.crci.2018.11.009.

9. Nabatipour, S., Mohammadi, S. & Mohammadi, A. (2020). Synthesis and comparison of two chromone based Schiff bases containing methoxy and acetamido substitutes as highly sustainable corrosion inhibitors for steel in hydrochloric acid. *J. Mol. Struc.* 1217(5), 128367. DOI: 10.1016/j.molstruc.2020.128367.

10. Chen, Y., Chen, Z. & Zhuo, Y. (2022). Newly synthesized morpholinyl mannich bases as corrosion inhibitors for N80 steel in acid environment. *Materials*. 15(12), 4218. DOI: 10.3390/MA15124218.

11. Wang, P., Gu, X., Wang, Q., Dong, J., Dong, S., Zhang, J., Zhu, S. & Chen, G. (2021). Corrosion inhibition of triazines in sulfur-containing oilfield wastewater. Desalinat. Water Treat. 235, 107–116. DOI: 10.5004/dwt.2021.27652.

12. Liu, Y., Chen, L., Tang, Y., Zhang, X. & Qiu, Z. (2022). Synthesis and characterization of nano-SiO_2@octadecylbisimidazoline quaternary ammonium salt used as acidizing corrosion inhibitor. *Rev. Adv. Mater. Sci*. 61(1), 186–194. DOI: 10.1515/rams-2022-0006.

13. Zhou, T., Yuan, J., Zhang, Z., Xin, X. & Xu, G. (2019). The comparison of imidazolium Gemini surfactant [C14-4-C14im]Br_2 and its corresponding monomer as corrosion inhibitors for A3 carbon steel in hydrochloric acid solutions: Experimental and quantum chemical studies. *Colloid. Surf*. A. 575, 57–65. DOI: 10.1016/j.colsurfa.2019.05.004.

14. Donahue, F.M. & Nobe, K. (1965). Theory of Organic Corrosion Inhibitors: Adsorption and Linear Free Energy Relationships. *J. Electrochem. Soc*. 112(9), 886. DOI: 10.1149/1.2423723.

15. Ahmed, S.K., Ali, W.B. & Khadom, A.A. (2018). Synthesis and characterization of new triazole derivatives as corrosion inhibitors of carbon steel in acidic medium. *J. Bio- and Tribo--Corrosion*, 35(4), 233–251. DOI: 10.1007/s40735-018-0209-1.

16. Hassan, H.H., Abdelghani, E. & Amin, M.A. (2007). Inhibition of mild steel corrosion in hydrochloric acid solution by triazole derivatives. *Electrochim. Acta.* 52(22), 6359–6366. DOI: 10.1016/j.electacta.2007.04.046.

17. Hosseini, M.G., Ehteshamzadeh, M. & Shahrabi, T. (2007). Protection of mild steel corrosion with Schiff bases in 0.5 M H_2SO_4 solution. *Electrochim. Acta*. 52(11), 3680–3685. DOI: 10.1016/j.electacta.2006.10.041.

18. Bai, Y., Zhang, J., Dong, S., Li, J., Zhang, R., Pu, C. & Chen, G. (2020). Effect of anion on the corrosion inhibition of cationic surfactants and a mechanism study. *Desalinat. Water Treat*. 188, 130–139. DOI: 10.5004/dwt.2020.25431.

19. Liu, Q., Gao, M., Zhang, J., Zhang, R., Li, J., Chen, S. & Chen, G. (2020). Synthesis and Interface Activity of Cetyltrimethylammonium Benzoate. *Russ. J. Phys. Chem. B+*. 14(1), 73–80. DOI: 10.1134/S1990793120010066.

20. Azhar, M.E., Mernari, B., Traisnel, M., Bentiss, F. & Lagrenée, M. (2001). Corrosion inhibition of mild steel by the new class of inhibitors [2,5-bis(N-pyridyl)-1,3,4-thiadiazoles] in acidic media. *Corros. Sci*. 43, 2229–2238. DOI: 10.1016/S0010--938X(01)00034-8.

21. Liu, P., Zhu, Y. & Zhao, L. (2020). New corrosion inhibitor for 13Cr stainless steel in 20% HCl solution. Anti--Corros. *Method. Mater.* 67(6), 557–564. DOI: 10.1108/ACMM-12-2019-2228.

22. Cui, M. & Li, X. (2021). Nitrogen and sulfur Co-doped carbon dots as ecofriendly and effective corrosion inhibitors for Q235 carbon steel in 1 M HCl solution. *RSC Adv*. 11(35), 21607–21621. DOI: 10.1039/d1ra02775a.

23. Yıldırım, A. & Çetin, M. (2008). Synthesis and evaluation of new long alkyl side chain acetamide, isoxazolidine and isoxazoline derivatives as corrosion inhibitors. *Corros. Sci*. 50(1), 155–165. DOI: 10.1016/j.corsci.2007.06.015.

24. Kumar, M.R., Mahendra, Y. & I.B., O. (2022). Electrochemical and computational investigation of adsorption and corrosion inhibition behaviour of 2-aminobenzohydrazide derivatives at mild steel surface in 15% HCl. *Mater. Chem. Phys*. 290(15), 126666. DOI: 10.1016/j.matchemphys.2022.126666.

25. Abd El-Aziz S., Fouda, Samir A., Abd El-Maksoud, Elsherbiny H. El-Sayed, Hazem A., Elbaz & Abousalem, A.S. (2021). Experimental and surface morphological studies of corrosion inhibition on carbon steel in HCl solution using some new hydrazide derivatives. *RSC Adv*. 11(22), 13497–13512. DOI: 10.1039/D1RA01405F.

26. Shetty, P. (2018). Hydrazide Derivatives: An Overview of Their Inhibition Activity against Acid Corrosion of Mild Steel. *S. Afr. J. Chem*. 71, 46–50. DOI: 10.17159/0379-4350/2018/v71a6.

27. Sunil, D., Kumari, P., Shetty, P. & Rao, S.A. (2022). Indole hydrazide derivatives as potential corrosion inhibitors for mild steel in HCl acid medium: experimental study and theoretical calculations. *T. Indian. I. Metals*. 75(1), 11–25. DOI: 10.1007/s12666-021-02382-8.

28. Siutkina, A.I., Sharavyeva, Y.O., Chashchina, S.V., Shipilovskikh, S.A. & Igidov, N.M. (2022). Synthesis and anti-inflammatory activity of N′-substituted 2-[2-(diarylmethylene) hydrazinyl]-5,5-dimethyl-4-oxohex-2-enehydrazides. *Russ. Chem. Bull.* 71(3), 496–501. DOI: 10.1007/s11172-022-3439-9.

29. Baleeva, N.S., Rybakov, V.B., Ivleva, E.A., Shiryaev, V.A. & Klimochkin, Y.N. (2020). Synthesis and chemical transformations of 7-Hydroxybicyclo[3.3.1]nonane-3-carbohydrazide. *Russ. J. Org. Chem*. 56(11), 1942–1951. DOI: 10.1134/S1070428020110081.

30. Liu, Q., Gao, M., Zhao, Y., Li, J., Qu, C., Zhang, J. & Chen, G. (2020). Synthesis and interfacial activity of a new quaternary ammonium surfactant as an oil/gas field chemical. *Tenside Surfact. Det.* 57(1), 90–96. DOI: 10.3139/113.110665.

31. Li, S., Guo, C., Wang, X., Guan, C. & Chen, G. (2022). Corrosion inhibition coating based on the self-assembled polydopamine films and its anti-corrosion properties. *Polymers* (Basel). 14(4), 794–807. DOI: 10.3390/polym14040794.

32. Elsharif, A.M., Abubshait, S.A., Abdulazeez, I. & Abubshait, H.A. (2020). Synthesis of a new class of corrosion inhibitors derived from natural fatty acid: 13□docosenoic acid amide derivatives for oil and gas industry. *Arab. J. Chem*. 13(5), 5363–5376. DOI: 10.1016/j.arabjc.2020.03.015.

33. Elsharif, A.M., Abubshait, S.A., Abdulazeez, I. & Abubshait, H.A. (2020). Synthesis, characterization and corrosion inhibition studies of polyunsaturated fatty acid derivatives on the acidic corrosion of mild steel: Experimental and computational studies. *J. Mol. Liq*. 319, 114162. DOI: 10.1016/j.molliq.2020.114162.

34. Elsharif, A.M. (2023). Synthesis and evaluation of newly E-octadec-9-enoic acid derivatives as sustainable corrosion inhibitors for mild steel in 1.0 M HCl. Arab. *J. Basic Appl. Sci*. 30(1), 26–46. DOI: 10.1080/25765299.2022.2164649.

35. Zhu, S., Li, Y., Wang, H., Li, J., Fu, A., Chen, G., Ma, D., Li, X. & Cheng, F. (2022). Corrosion resistance mechanism of mica-graphene/epoxy composite coating in CO_2-Cl^- system. *Materials*. 15(3), 1194. DOI: 10.3390/ma15031194.

36. Chaouiki, A., Lgaz, H., Salghi, R., Gaonkar, S.L., Bhat, S.K., Jodeh, S., Toumiat, K. & Oudda, H. (2019). New benzohydrazide derivative as corrosion inhibitor for carbon steel in a 1.0 M HCl solution: Electrochemical, DFT and monte carlo simulation studies. *Portugaliae Electrochim. Acta*. 37(3), 147–165. DOI: 10.4152/PEA.201903147.

37. Alarfaji, S., Ali, I., Bani-Fwaz, M. & Bedair, M. (2021). Synthesis and assessment of two malonyl dihydrazide derivatives as corrosion inhibitors for carbon steel in acidic media: Experimental and theoretical studies. *Molecules* (Basel, Switzerland). 26(11), 3138–3155. DOI: 10.3390/molecules26113183.

38. Lingjian, K. & Mingyang, Z. (2022). Adsorption of methylene blue on chestnut shell-based activated carbon: Calculation of thermodynamic parameters for solid-liquid interface adsorption. *Catalysts*. 12(8), 813–823. DOI: 10.3390/catal12080813.

39. Lin, J., Liu, Q., Zhang, J., Wu, Y., Li, H., Ma, Y., Qu, C., Song, W. & Chen, G. (2019). Corrosion inhibition and structure-efficiency relationship study of CTAC and CDHAC. *Desalinat. Water Treat*. 1391–1396. DOI: 10.5004/dwt.2019.23269.

40. Khandelwal, R., Sahu, S. & Arora, S. (2018). Comparative study of Schiff's bases and plant extract as corrosion inhibitors. *Adv. Sci. Engin. Med.* 10(10), 1023–1028. DOI: 10.1166/asem.2018.2198.

41. Gu, X., Zhang, H., Zhang, Z., Du, W., Zhu, S. & Chen, G. (2021). Modification and application of walnut peel extract as acidic corrosion inhibitor. *J. Biobased. Mater. Bio.* 15(6), 820–825. DOI: 10.1166/jbmb.2021.2138.

42. Herrag, L., Hammouti, B., Elkadiri, S., Aouniti, A., Jama, C., Vezin, H. & Bentiss, F. (2010). Adsorption properties and inhibition of mild steel corrosion in hydrochloric solution by some newly synthesized diamine derivatives: Experimental and theoretical investigations. *Corros. Sci*. 52(9), 3042–3051. DOI: 10.1016/j.corsci.2010.05.024.

43. Obi-Egbedi, N.O. & Obot, I.B. (2011). Inhibitive properties, thermodynamic and quantum chemical studies of alloxazine on mild steel corrosion in H_2SO_4. *Corros. Sci.* 53(1), 263–275. DOI: 10.1016/j.corsci.2010.09.020.

44. Elsharif, A.M. (2023). Newly synthesized nanohybrids based on gallic acid derivatives for pipeline steel corrosion in hydrochloride acid medium. Prog. Org. Coat., 185, 107869. DOI: 10.1016/j.porgcoat.2023.107869.

45. Xu, Z., Cao, X., Wang, Y., Slaný, M., Unčík, S., Li, S. & Tang, Y. (2023). Effective corrosion inhibitor of mild steel

in marine environments: Synthesis and application of hydrazides. *Sustainable Mater. Tech*. 38, e00747. DOI: 10.1016/j.susmat.2023.e00747.

46. Gao, M., Zhang, J., Liu, Q., Li, J., Zhang, R. & Chen, G. (2019). Effect of the alkyl chain of quaternary ammonium cationic surfactants on corrosion inhibition in hydrochloric acid solution. *Comptes Rendus Chim*. 22(5), 355–362. DOI: 10.1016/j.crci.2019.03.006.

47. John, S., Kuruvilla, M. & Joseph, A. (2012). Surface morphological and impedance spectroscopic studies on the interaction of polyethylene glycol (PEG) and polyvinyl pyrrolidone (PVP) with mild steel in acid solutions. *Res. Chem. Intermed*. 39(3), 1169–1182. DOI: 10.1007/s11164-012-0675-x.

48. Shaban, S.M., Elbhrawy, M.F., Fouda, A.S., Rashwan, S.M., Ibrahim, H.E. & Elsharif, A.M. (2021). Corrosion inhibition and surface examination of carbon steel 1018 via N-(2-(2-hydroxyethoxy)ethyl)-N,N-dimethyloctan-1-aminium bromide in 1.0 M HCl. *J. Mol. Struct.* 1227. DOI: 10.1016/j.molstruc.2020.129713.

49. Cai, K., Zuo, S., Luo, S., Yao, C., Liu, W., Ma, J., Mao, H. & Li, Z. (2016). Preparation of polyaniline/graphene composites with excellent anti-corrosion properties and their application in waterborne polyurethane anticorrosive coatings. *RSC Adv*. 6(98), 95965–95972. DOI: 10.1039/C6RA19618G.